PAPER

Check for updates

Towards biodegradable conducting polymers by incorporating seaweed cellulose for decomposable wearable heaters†

Mei Ying Teo, [ID] [a] Keemi Lim,[b] Kean C. Aw,[a] Seyoung Kee*[c] and Jonathan Stringer*[a]

Thermotherapy shows significant potential for pain relief and enhanced blood circulation in wildlife rehabilitation, particularly for injured animals. However, the widespread adoption of this technology is hindered by the lack of biodegradable, wearable heating pads and concerns surrounding electronic waste (E-waste) in natural habitats. This study addresses this challenge by investigating an environmentally-friendly composite comprising poly(3,4-ethylenedioxythiophene):polystyrene sulfonate (PEDOT:PSS), seaweed cellulose, and glycerol. Notably, this composite exhibits remarkable biodegradability, losing half of its weight within one week and displaying noticeable edge degradation by the third week when placed in soil. Moreover, it demonstrates impressive heating performance, reaching a temperature of 51 °C at a low voltage of 1.5 V, highlighting its strong potential for thermotherapy applications. The combination of substantial biodegradability and efficient heating performance offers a promising solution for sustainable electronic applications in wildlife rehabilitation and forest monitoring, effectively addressing the environmental challenges associated with E-waste.

Introduction

Wearable heaters are essential in thermotherapy for generating and controlling heat, offering benefits such as improved blood circulation, reduced inflammation, and pain relief, while also enhancing the healing process of wounds by promoting the movement of active materials through the skin.[1–3] Currently, most wearable heaters are made of metal nanowires, conducting polymers, carbon-based nanomaterials, and liquid metals, frequently combined with substrates like fabric or elastomers.[4–8] However, a significant issue with these wearable heaters is their non-biodegradable and environmentally unfriendly, which further exacerbates the problem of electronic waste (E-waste) alongside the increasing prevalence of wearable electronics.[9] In pursuing of a greener and cleaner planet, it is crucial to prioritise the development of electronics that utilize

environmentally friendly materials and processes capable of natural decomposition over time. This approach mitigates the E-waste problem and unlocks potential for non-invasive wildlife monitoring and the exploration of uninhabited areas, with minimal environmental impact.[10,11]

A solution-processable conducting polymer, poly(3,4-ethylenedioxythiophene):polystyrene sulfonate (PEDOT:PSS) is regarded as the most successful conducting polymer for practical applications due to its remarkable properties, including high electrical conductivity, eco-friendly aqueous processability, and good stability in different environmental conditions.[12–15] These exceptional characteristics have paved the way for the development of advanced organic electronic devices such as organic solar cells, organic light-emitting diodes, organic transistors, and bioelectronics applications.[12,16,17] In response to the increasing demand for wearable and portable electronics, considerable attention has been directed towards improving the insufficient mechanical flexibility/stretchability of PEDOT:PSS *via* the incorporation of plasticizers, elastomeric materials, and/or soft polymers.[18,19] Moreover, several research groups have begun exploring the potential of fabricating biocompatible PEDOT:PSS hydrogel for bioelectronics, inspired by the fact that an increase in ionic strength can help in the gelation of PEDOT:PSS aqueous dispersions.[12,20,21]

Recently, biodegradable and environmentally friendly electronics have become a hot topic due to the increased awareness of E-waste and its environmental impact.[9] Although PEDOT:PSS exhibits excellent electronic properties through the aforementioned processing and treatments, developing PEDOT:PSS with

aDepartment of Mechanical Engineering, The University of Auckland, Symonds Street, Auckland, 1010, New Zealand. E-mail: j.stringer@auckland.ac.nz

bDepartment of Chemical and Materials Engineering, The University of Auckland, Symonds Street, Auckland, 1010, New Zealand

cDepartment of Polymer Engineering, Pukyong National University, Busan 48513, Republic of Korea. E-mail: sykee@pknu.ac.kr

† Electronic supplementary information (ESI) available: Photograph of a non-homogeneous PEDOT:PSS/glycerol (Fig. S1), TGA for PEDOT:PSS, s-cellulose and PEDOT:PSS composite film (Fig. S2), setup for the degradation experiment (Fig. S3), the estimated number of days required for the complete degradation (Fig. S4), photograph of a setup used to measure the heating performance (Fig. S5), heating DI water with PEDOT:PSS composite film (Fig. S6). See DOI: https://doi.org/10.1039/d3ra04927b

biodegradable feature has been a challenging issue for its environmental-friendly applications.[13,22] Earlier research has proposed that composite materials, combining electronically active polymers with biodegradable materials, offer a promising sustainable and environmentally friendly solution.[23,24] These composites can maintain electronic capabilities while naturally breaking down, offering enhanced biodegradability without compromising electronic properties. One of the first demonstrations of biodegradable PEDOT:PSS was reported in 2016, where silk was selected as the biodegradable counterpart and subjected to be enzymatically degraded.[25] Subsequent studies have confirmed that the feasibility of combining PEDOT:PSS and silk, and achieving degradation *via* enzymatic or alcohol solutions.[26,27] More recently, researchers have explored incorporating clay with PEDOT:PSS to enhance biodegradability, in which super worms can ingest the composite for degradation.[28] On the other hand, while there have been studies on PEDOT:PSS composite films with cellulose, most studies have utilised low-dose toxicity solvents (*e.g.*, dimethyl sulfoxide) as conductivity enhancer and no comprehensive degradation studies have been studied so far.[29–33] Therefore, further study is needed to understand the characteristics of this composite system using only environmentally friendly materials and explore its biodegradability, marching towards the green electronics in the future.

For this reason, we conducted a study on the PEDOT:PSS composite system consisting of PEDOT:PSS, seaweed cellulose (s-cellulose) and glycerol, and assessed its biodegradability over time using soil as a medium. The s-cellulose was chosen due to its natural abundance, biocompatibility, biodegradability, and nontoxicity.[3,34,35] We hypothesise that the addition of s-cellulose can enhance the overall biodegradability of the PEDOT:PSS composite. Glycerol, knows as a plasticizer and secondary dopant for PEDOT:PSS, was utilised to improve its electrical conductivity.[36–39] As a result, the combination of these PEDOT:PSS, s-cellulose and glycerol led to the development of highly conductive and biodegradable organic conductors. We have successfully developed heaters using these composite films. Due to their biodegradable nature, these heaters have the potential for thermotherapy applications, including use in wildlife rehabilitation. They also hold promise for applications such as defrosting and de-icing plants and serving as heating pads to stimulate seed germination during cold weather conditions.

Results and discussion

Fabrication of PEDOT:PSS composite films

The fabrication process of PEDOT:PSS/s-cellulose/glycerol composite films is depicted in Fig. 1, aimed at enhancing the overall biodegradability of PEDOT:PSS by incorporating s-cellulose. Glycerol plays a multifunctional role in this process, acting as a plasticizer to improve the mechanical properties by forming hydrogen bonds not only with s-cellulose chains but also with PSS⁻ chains. This thus disrupts the original hydrogen bonds among s-cellulose chains and PSS⁻ chains, which results in well-mixed composite.[40] Additionally, glycerol serves as an

additive enhancing the electrical conductivity of PEDOT:PSS, promoting agglomeration and gelation of the material during drying to obtain highly conductive free-standing PEDOT:PSS composite films.[37,38] To produce these biodegradable electrical films, a mixture of PEDOT:PSS, s-cellulose, and glycerol are prepared in 10 : 5 : 8 (ml) ratio. The selection of 5 ml of s-cellulose is crucial to ensure the formation of a homogeneous film without segregation and precipitation, as demonstrated in ESI (ESI) Fig. S1.† The mixture solution is subjected to magnetic stirring until it reaches a state of homogeneity, after which it is cast into a 55 mm diameter Petri dishes and dried in an oven at 60 °C for two days. Following the drying process, the films can be easily peeled off from the Petri dishes, facilitated by the hygroscopic nature of glycerol, which helps maintain the wet stability of the composite films. Subsequently, the films are further dried on a hotplate at 120 °C. As a result, we successfully achieved highly flexible conductive PEDOT:PSS composite films.

Electrical properties of PEDOT:PSS composite films

To evaluate the electrical performance of the PEDOT:PSS composite films, the electrical conductivity was compared with the pure PEDOT:PSS, which was measured using a four-point-probe. The obtained average conductivity of pure PEDOT:PSS films is 0.7 S cm⁻¹ and that of PEDOT:PSS composite films is 5.3 S cm⁻¹, an order higher than pure PEDOT:PSS after the introduction of s-cellulose and glycerol. This notable increase in conductivity can be attributed to the formation of hydrogel bonds between the hydroxyl groups of glycerol and PSS⁻.[40] These bonds weaken the coulombic attraction between PEDOT and PSS, promoting the rearrangement of PEDOT chains with a more extended conformation.[41] This conformational change allows for enhanced π–π interactions between PEDOT chains, creating more conductive pathways for efficient charge transport.

To confirm that, we conducted Raman spectroscopy analysis for pure PEDOT:PSS, PEDOT:PSS/s-cellulose, PEDOT:PSS/glycerol, and PEDOT:PSS/s-cellulose/glycerol, as depicted in Fig. 2a. In the Raman spectra, the band observed between 1400 and 1500 cm⁻¹ are attributed to PEDOT, with a characteristic peak at 1432 cm⁻¹ for pure PEDOT, corresponding to symmetrical $C_\alpha = C_\beta$ stretching vibrations of the aromatic rings in PEDOT.[22] Notably, we observed a significant red shift from 1432 cm⁻¹ to 1428 cm⁻¹ with the addition of s-cellulose and further to 1425 cm⁻¹ with the addition of glycerol. This shift indicates a transformation of PEDOT chains from a coil-like (benzenoid-dominant) to linear-like (quinoid-dominant) structure, enabling greater delocalisation of conjugated π-electrons along the chains. Consequently, this conformational change can enhance the conductivity of PEDOT:PSS. Furthermore, it is worth noting that the conformational change is more pronounced with the addition of glycerol compared to s-cellulose, indicating that the primary increase in conductivity is attributed to glycerol, which is in a good agreement with the previous report for PEDOT:PSS/s-cellulose.[31]

Pure PEDOT:PSS and PEDOT:PSS composite film were used as electrical conductor in an LED circuit to demonstrate their
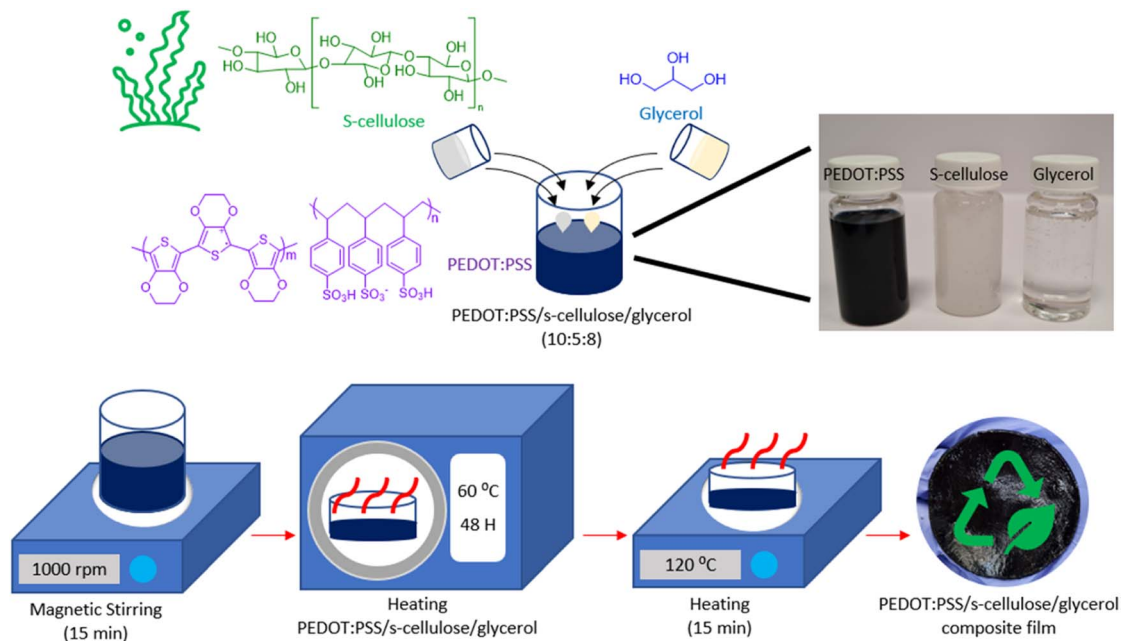
Fig. 1 Schematic illustration of the preparation of PEDOT:PSS/s-cellulose/glycerol composite films with chemical structure of PEDOT:PSS, s-cellulose and glycerol.

electrical conductivities. The PEDOT:PSS composite film demonstrates higher LED luminescence compared to the pure PEDOT:PSS film, highlighting its superior conductivity when serving as a better conductor (Fig. 2b). Additionally, the mechanical robustness and flexibility of the PEDOT:PSS composite films were assessed. The films exhibited the ability to bend, fold, and twist while maintaining the LED light functionality. Furthermore, it can adhere conformably to human skin, showcasing its excellent conformability and deformability. Notably, the addition of s-cellulose and glycerol is essential to achieve thick films with more than several tens of microscale thickness, enabling various applications with free-standing feature (Fig. 2c).

Microstructural and chemical characteristics of PEDOT:PSS composite films

The scanning electron microscope (SEM) images in Fig. 3 compare the surface morphologies of pure PEDOT:PSS, PEDOT:PSS with glycerol, pure s-cellulose and composite films. The pure PEDOT:PSS film shows the typical smooth and homogenous surface (Fig. 3a). On the other hand, the introduction of glycerol into PEDOT:PSS results in the formation of interconnected micro grains that exhibit a highly clustered structure (Fig. 3b). The interconnected clustered grains, linking conducting islands, facilitate the charge transfer between PEDOT chains, enhancing PEDOT:PSS conductivity.[42] These observation is in line with the Raman spectra analysis, providing further evidence of the positive effect of glycerol on the conductivity of PEDOT:PSS. In the surface morphology of the PEDOT:PSS composite films, it seems that the fibrillar-structure mainly originating from s-cellulose were well

distributed on the surface of the PEDOT:PSS, confirming the uniform presence of s-cellulose in the composite films (Fig. 3c and d).

To confirm that s-cellulose and glycerol are present in the films upon the fabrication, we performed attenuated total reflection Fourier-transform infrared spectroscopy (ATR-FTIR) by comparing the presence of the absorption bands with the pure components (Fig. 4). In the ATR-FTIR spectra, we successfully identified PEDOT:PSS, s-cellulose, and glycerol in the composite films by their characteristic peaks. The fingerprint region of PEDOT:PSS appears in the range of 500–1000 cm^{-1}.[43,44] The broad band at 3000–3500 cm^{-1}, 2800–3000 cm^{-1}, and the peak at 1030 cm^{-1} are assigned to O–H stretching, C–H stretching, C–O stretching from glycerol.[45,46] Additionally, the peak at 3338 cm^{-1} and 1647 cm^{-1} are related to O–H stretching and bending in s-cellulose.[47,48] This result indicates the formation of a composite between PEDOT:PSS, s-cellulose, and glycerol.

Thermal degradation and biodegradability of PEDOT:PSS composite films

To investigate the temperature-dependent thermal property changes in PEDOT:PSS after adding s-cellulose and glycerol, thermogravimetric analysis (TGA) was performed on PEDOT:PSS, s-cellulose and composite films (ESI, Fig. S2†). In all samples, the weight loss at around 100 °C can be attributed to water evaporation within the films. The pure PEDOT:PSS film exhibits significant thermal degradation at approximately 300 °C due to the decomposition of PSS, resulting from degradation of the sulfonate group in styrene, while decomposition of the PEDOT:PSS polymer backbones likely occurs above 350 °C.[49] The pure s-cellulose film shows a sharp weight loss starting
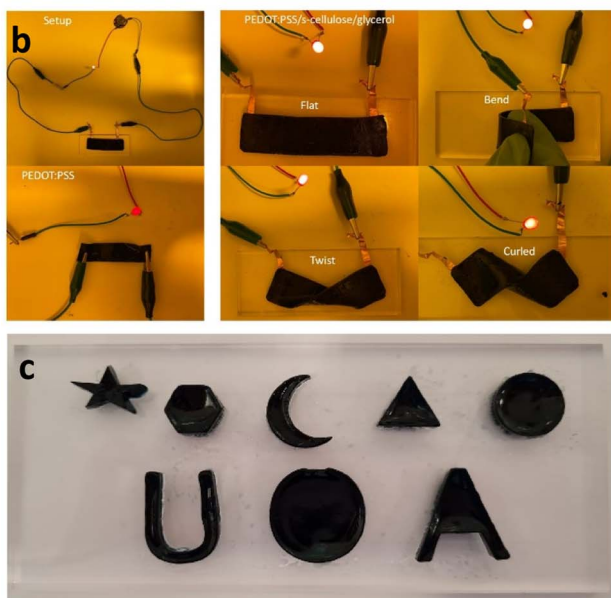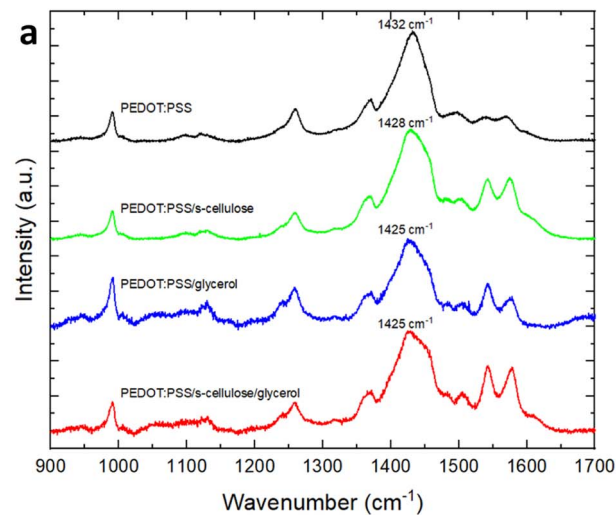
Fig. 2 (a) Raman spectra of PEDOT:PSS and with s-cellulose, with glycerol, and PEDOT:PSS composite films. (b) Photograph of an LED integrated circuit connected to an electrode. A dimmed LED with pure PEDOT:PSS serving as the conductor. Next, a bright LED with PEDOT:PSS composite films serving as the conductor under various conditions. (c) Photograph of PEDOT:PSS composite with various shapes.
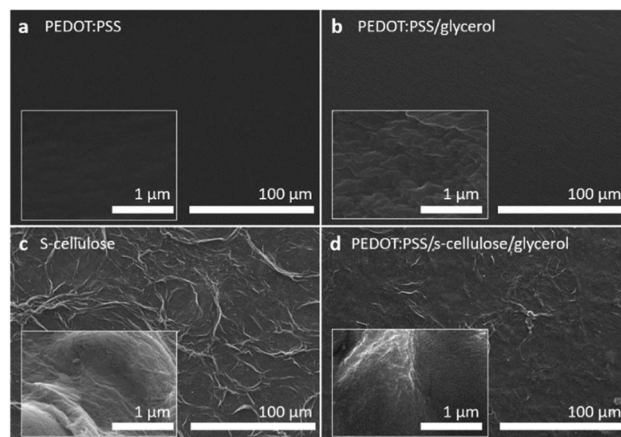

Fig. 3 (a) PEDOT:PSS (b) PEDOT:PSS/glycerol (c) s-cellulose and (d) PEDOT:PSS composite film.
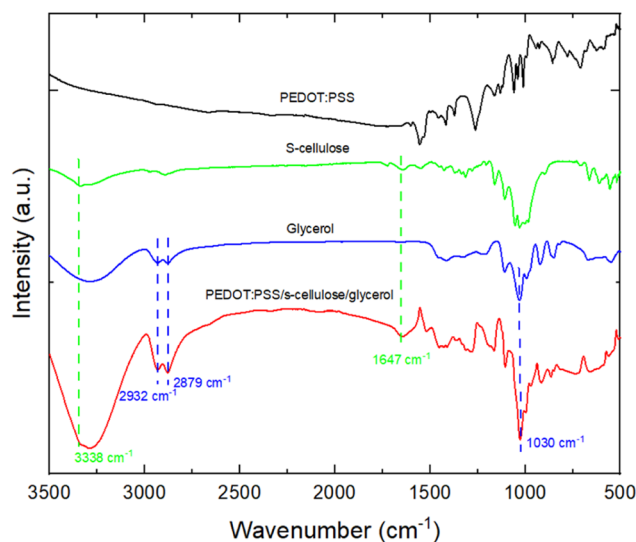
Fig. 4 ATR-FTIR spectroscopy for PEDOT:PSS, s-cellulose, glycerol, and PEDOT:PSS composite film.

around 250 °C. In the case of the PEDOT:PSS composite film, the decomposition and weight loss commence earlier, from 130 to 240 °C, mainly due to the vaporisation of glycerol.[46] These findings, along with ATR-FTIR analysis, clearly verify the presence of glycerol and s-cellulose in the composite films. More importantly, the addition of s-cellulose and glycerol to PEDOT:PSS accelerates thermal degradation, which is advantageous for biodegradable characteristics.

S-cellulose is widely recognized as biodegradable material. We aimed to assess the biodegradability of PEDOT:PSS composite films by evaluating their degradation rate in soil. The experimental setup, as depicted in ESI, Fig. S3,† involved

exposing the films to simulated sunlight for several hours each day. The weight *versus* day graph displays a significant reduction in the film's weight, with almost a 50% decrease after one week (Fig. 5). This can be attributed to the loss of water and glycerol into the soil, which is evident from the thinner appearance and dried surface of the PEDOT:PSS composite films. Additionally, the consistently moist soil without the need for additional watering further confirms the presence of glycerol in the soil, as glycerol naturally retains water. Subsequently, the weight reduction occurred at a slower pace in the following weeks. Notably, we observed the formation of holes and cracks along the edges of one film during the third week in the soil. Similar deterioration was observed for another sample during the seventh week, with both samples continuing to degrade in subsequent weeks. Overall, this soil degradation provides compelling evidence that the biodegradability of PEDOT:PSS films can be enhanced by incorporating s-cellulose. Based on
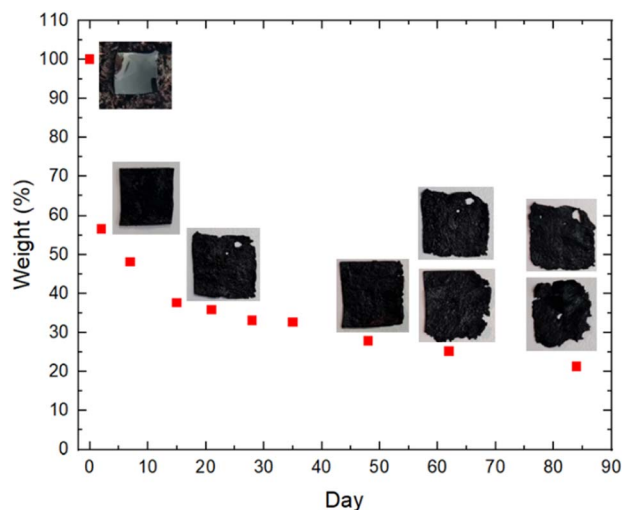
Fig. 5 Degradation of PEDOT:PSS composite films over time in soil (n = 3).

our observations, we estimate that complete degradation of the films in soil conditions would occur after approximately 460 days (ESI, Fig. S4†).

Application as a biodegradable electrical heater

The PEDOT:PSS composite films exhibit excellent electrothermal properties suitable for thermal therapy applications in wearable

and portable heaters (Fig. 6). The circular PEDOT:PSS composite films with a diameter of 55 mm were connected to a direct current (DC) power supply through copper tape placed on 1 mm-thick glass supporting substrate, and supplied with voltages ranging from 1.0 to 3.5 V (ESI, Fig. S5†). All PEDOT:PSS composite films were tested in a temperature-controlled environment (set at 25 °C and 1 atm) and the temperature distribution on the films surface was captured using a thermal IR camera. The electrothermal performance of the PEDOT:PSS composite heaters was evaluated under three key parameters, maximum operating temperature, heating time, and cooling time.

Fig. 6a shows the relationship between surface temperature and applied DC voltage for PEDOT:PSS composite films as electrical heaters. As the DC voltage increases from 0 V to 3.5 V, the temperature of the film rises from 23 °C to 105 °C. The temperature was measured after applying voltages for two minutes. The mechanism underlying the heating of PEDOT:PSS composite films under applied voltages involves current flow through the composite. Specifically, some of the kinetic energy from the flowing electrons is converted into heat, thereby warming the PEDOT:PSS composite film.[50] In addition, this result also demonstrates the effectiveness of conversion of electrical energy into Joule heating due to the low resistance as the current allows to flow through the PEDOT:PSS composite films.[51] As a demonstration of the heater's capability, we used PEDOT:PSS composite to heat up deionized water (ESI, Fig. S6†).

Next, we examined the time-dependent temperature profiles for the PEDOT:PSS composite films under different voltage
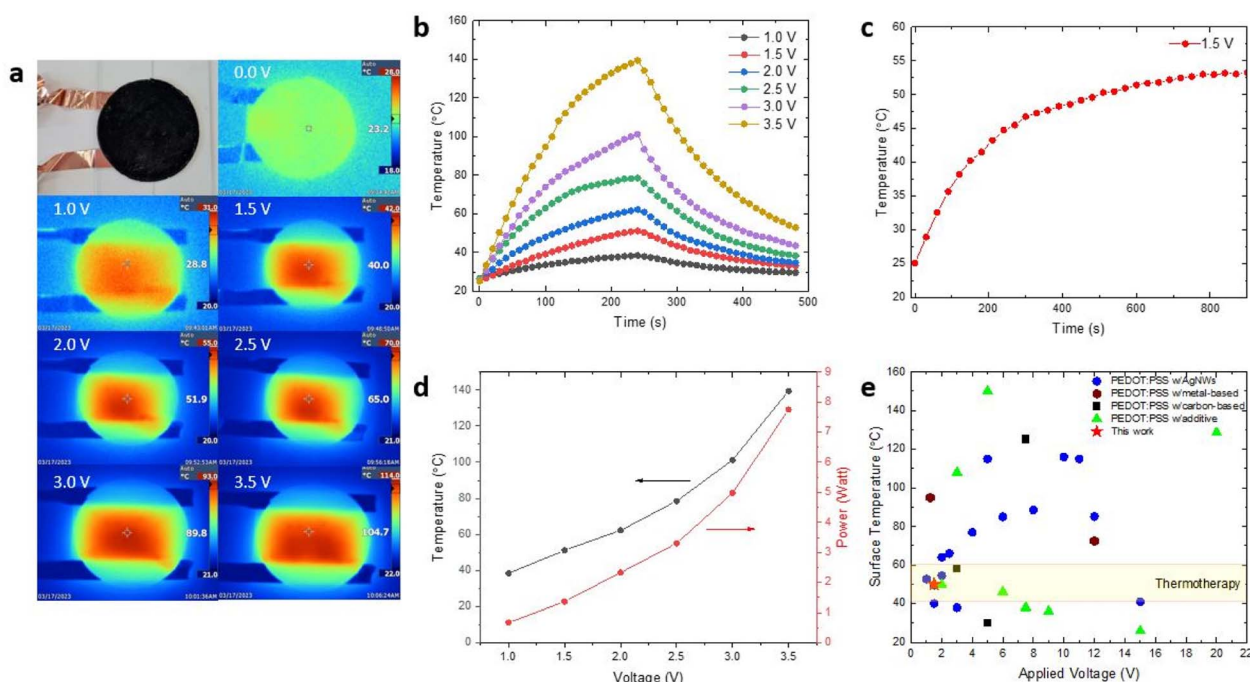

Fig. 6 Joule heating characterisation of PEDOT:PSS composite films as a wearable and portable heater (a) photography of PEDOT:PSS composites where the surface temperature was monitored two minutes after applying the corresponding voltage. (b) Time-dependent temperature profile of the heater against various voltages. (c) Thermal stability curve of the heater showing stable performance for 15 min. (d) Relationship between temperature and power consumption of the heater with various voltages. (e) Comparison of the performance of the fabricated PEDOT:PSS composite heaters from the literature and this work.

applies (Fig. 6b). The temperature gradually rises as both the operating voltage and time increase. For instance, after two minutes, the samples operated at lower voltages of 1 V and 1.5 V reach their highest heating state temperatures of 38 °C and 51 °C. By increasing the driven voltages to 2.0 V and 2.5 V, the surface temperature of the samples reaches maxima of 62 °C and 79 °C, respectively. Similarly, when operated at higher voltages of 3.0 V and 3.5 V, the samples reach surface temperatures of 101 °C and 139 °C, respectively. Subsequently, upon turning off the applied voltage, these samples exhibit a rapid cooling response with the rate of cooling primarily influenced by the highest temperature and decrease swiftly as the accumulated heat dissipates into the surrounding environment through convection. Furthermore, it is worth noting that the temperature plateau was not achieved during the 240 s heating time due to the large heat capacity of the 1 mm-thick glass substrate used to support the PEDOT:PSS composite films in this experiment. The heat conducts from the PEDOT:PSS composite film into the supporting substrate resulting in significant heat storage, which can impact the rapid increase in temperature. When the power supply was turned off, the stored heat from the substrate began to conduct back into the film, also affecting the rapid decrease in temperature. The achievement of a temperature plateau could be addressed by utilizing thinner substrates for testing, although it was not the primary focus of this experiment.[52] Overall, modulating the applied DC voltage enables precise temperature control to meet specific usage demands, showcasing the outstanding electrothermal characteristics of PEDOT:PSS composite films for Joule heating applications.

Considering the safe operation and compatibility for wearable applications, 1.5 V was chosen as the applied voltage to study the long-term heating stability of the PEDOT:PSS composite films. At 1.5 V, the PEDOT:PSS composite films demonstrate good thermal stability and provide reliable heating performance for 900 s (Fig. 6c). The conductive PEDOT:PSS networks provide current pathway in the composite films, enabling stable and efficient heat generation even at a low voltage of 1.5 V. This heating stability is highly desirable for long-term and reliable operation of the heater during deployment. Fig. 6d illustrates the surface temperature increase as a function of applied voltage, with low power consumption ranging from 0.6 to 7.7 watts across the driving voltages of 1 V to 3.5 V. This corresponds to a temperature range of 38 to 139 °C.

Furthermore, Fig. 6e compares the Joule heating performance of various PEDOT:PSS-based electrical heaters with silver nanowires (AgNWs),[5,52–65] metals,[51,66] carbon based[67–69] and additives.[6,36,70–75] Among these, AgNWs are the most commonly combined with PEDOT:PSS to form composite for wearable heaters. This is due to their high electrical and thermal conductivities, which enable efficient heat generation.[53,54] However, these nanomaterials are prone to oxidation because of their high surface-to-volume ratio, not to mention the high raw material costs.[53] PEDOT:PSS composites that incorporate metals or carbon based materials typically require a substrate. Such substrate might not adequately soft to adapt to skin for wearable applications, nor biodegradable.[51,67] To enhance

wearer comfort, fabric-like wearable heaters have also been developed, primarily using PEDOT:PSS on textiles.[6,36,70,72–75] However, these too are not biodegradable. Our PEDOT:PSS composite heaters can achieve high temperature under relatively low operating voltage, demonstrating its superior performance as low-voltage wearable and portable heaters when compared to those heaters reported in the previous literature. Additionally, its flexibility and importantly biodegradability, make them ideal for thermotherapy applications in wound healing and pain management for injured wildlife without worrying E-waste in the forest. Furthermore, its excellent heating capability and biodegradability make it applicable for defrosting, deicing, demisting, and promoting seed germination in cold weather regions.

Conclusions

We have studied electrical, morphology, chemical, biodegradation and heating properties of PEDOT:PSS upon the addition of s-cellulose and glycerol. The addition of s-cellulose and glycerol improved the electrical conductivity, thermal stability, and biodegradability of PEDOT:PSS. As confirmed by Raman spectroscopy, glycerol acts as a plasticizer, enhancing the films' mechanical properties and conductivity. The SEM-based morphological analysis revealed glycerol-assisted interconnected micrograins that promoted charge transfer in PEDOT:PSS. The PEDOT:PSS composite films exhibited accelerated thermal degradation and enhanced biodegradability in soil tests, indicative of their potential as eco-friendly conductors. They also demonstrated excellent electrothermal performance, achieving high surface temperatures under low operating voltages. Overall, this research contributes to the development of sustainable and eco-friendly materials for electronic and thermal applications, paving the way for establishing biodegradable and environmentally friendly electronics and future technologies.

Author contributions

Mei Ying Teo: writing, methodology, investigation, conceptualisation. Keemi Lim: ATR-FTIR, TGA measurement and reviewing manuscript. Kean C. Aw: conceptualisation and reviewing manuscript. Seyoung Kee: conceptualisation and reviewing manuscript. Jonathan Stringer: conceptualisation and reviewing manuscript.

Conflicts of interest

There are no conflicts to declare.

Acknowledgements

Notes and references

1 S. Lee, S. W. Kim, M. Ghidelli, H. S. An, J. Jang, A. L. Bassi, S. Y. Lee and J. U. Park, *Nano Lett.*, 2020, **20**, 4872–4881.

2 J. Liu, J. Li, Z. Wu, S. Xu, C. Wan and X. Huang, *Adv. Mater. Technol.*, 2023, 2202159.

3 D. S. Lakshmi, N. Trivedi and C. R. K. Reddy, *Carbohydr. Polym.*, 2017, **157**, 1604–1610.

4 P. Ilanchezhiyan, A. S. Zakirov, G. M. Kumar, S. U. Yuldashev, H. D. Cho, T. W. Kang and A. T. Mamadalimov, *RSC Adv.*, 2015, **5**, 10697–10702.

5 L. Li, B. Sun, W. Li, L. Jiang, Y. Zhou, J. Ma, S. Chen, X. Ning and F. L. Zhou, *Macromol. Mater. Eng.*, 2021, **306**, 2100365.

6 M. A. Jalil, A. Ahmed, M. M. Hossain, B. Adak, M. T. Islam, M. Moniruzzaman, M. S. Parvez, M. Shkir and S. Mukhopadhyay, *ACS Omega*, 2022, **7**, 12716–12723.

7 R. Wang, Z. Xu, J. Zhuang, Z. Liu, L. Peng, Z. Li, Y. Liu, W. Gao, C. Gao, R. Wang, Z. Xu, J. Zhuang, Z. Liu, L. Peng, Z. Li, Y. Liu, W. Gao and C. Gao, *Adv. Electron. Mater.*, 2017, **3**, 1600425.

8 Y. Wang, Z. Yu, G. Mao, Y. Liu, G. Liu, J. Shang, S. Qu, Q. Chen and R. W. Li, *Adv. Mater. Technol.*, 2019, **4**, 1800435.

9 M. Heacock, C. B. Kelly, K. A. Asante, L. S. Birnbaum, Å. L. Bergman, M. N. Bruné, I. Buka, D. O. Carpenter, A. Chen, X. Huo, M. Kamel, P. J. Landrigan, F. Magalini, F. Diaz-Barriga, M. Neira, M. Omar, A. Pascale, M. Ruchirawat, L. Sly, P. D. Sly, M. van den Berg and W. A. Suk, *Environ. Health Perspect.*, 2015, **124**, 550–555.

10 F. Wiesemuller, A. Miriyev and M. Kovac, *AIRPHARO 2021 – 1st AIRPHARO Workshop on Aerial Robotic Systems Physically Interacting with the Environment*, DOI: DOI: 10.1109/AIRPHARO52252.2021.9571067.

11 M. Baratchi, N. Meratnia, P. J. M. Havinga, A. K. Skidmore and B. A. G. Toxopeus, *Sensors*, 2013, **13**, 6054–6088.

12 V. R. Feig, H. Tran, M. Lee and Z. Bao, *Nat. Commun.*, 2018, **9**, 1–9.

13 N. Kim, S. Kee, S. H. Lee, B. H. Lee, Y. H. Kahng, Y. R. Jo, B. J. Kim and K. Lee, *Adv. Mater.*, 2014, **26**, 2268–2272.

14 H. Kang, S. Jung, S. Jeong, G. Kim and K. Lee, *Nat. Commun.*, 2015, **6**, 1–7.

15 H. Kang, S. Hong, J. Lee, K. Lee, H. Kang, S. Hong, J. Lee and K. Lee, *Adv. Mater.*, 2012, **24**, 3005–3009.

16 H. Kang, S. Kee, K. Yu, J. Lee, G. Kim, J. Kim, J.-R. Kim, J. Kong, K. Lee, H. Kang, S. Kee, K. Yu, J. Lee, G. Kim, J. Kim, J. Kim, J. Kong and K. Lee, *Adv. Mater.*, 2015, **27**, 1408–1413.

17 S. Kee, N. Kim, B. Park, B. S. Kim, S. Hong, J. H. Lee, S. Jeong, A. Kim, S. Y. Jang and K. Lee, *Adv. Mater.*, 2018, **30**, 1703437.

18 M. Y. Teo, N. Kim, S. Kee, B. S. Kim, G. Kim, S. Hong, S. Jung and K. Lee, *ACS Appl. Mater. Interfaces*, 2017, **9**, 819–826.

19 L. V. Kayser and D. J. Lipomi, *Adv. Mater.*, 2019, **31**, 1806133.

20 M. A. Leaf and M. Muthukumar, *Macromolecules*, 2016, **49**, 4286–4294.

21 M. Y. Teo, N. Ravichandran, N. Kim, S. Kee, L. Stuart, K. C. Aw and J. Stringer, *ACS Appl. Mater. Interfaces*, 2019, **11**, 37069–37076.

22 J. Ouyang, C. W. Chu, F. C. Chen, Q. Xu and Y. Yang, *Adv. Funct. Mater.*, 2005, **15**, 203–208.

23 J. Xie, M. R. MacEwan, A. G. Schwartz and Y. Xia, *Nanoscale*, 2010, **2**, 35–44.

24 J. Y. Lee, C. A. Bashur, A. S. Goldstein and C. E. Schmidt, *Biomaterials*, 2009, **30**, 4325–4335.

25 R. K. Pal, A. A. Farghaly, C. Wang, M. M. Collinson, S. C. Kundu and V. K. Yadavalli, *Biosens. Bioelectron.*, 2016, **81**, 294–302.

26 A. Zhuang, X. Huang, S. Fan, X. Yao, B. Zhu and Y. Zhang, *ACS Appl. Mater. Interfaces*, 2022, **14**, 123–137.

27 S. Pradhan and V. K. Yadavalli, *ACS Appl. Electron. Mater.*, 2021, **3**, 21–29.

28 S. Lee, Y. Hong and B. S. Shim, *Adv. Sustainable Syst.*, 2022, **6**, 2100056.

29 H. Du, M. Zhang, K. Liu, M. Parit, Z. Jiang, X. Zhang, B. Li and C. Si, *Chem. Eng. J.*, 2022, **428**, 131994.

30 J. W. Han, A. F. Wibowo, J. Park, J. H. Kim, A. Prameswati, S. A. N. Entifar, J. Lee, S. Kim, D. Chan Lim, M. W. Moon, M. S. Kim and Y. H. Kim, *Org. Electron.*, 2022, **105**, 106499.

31 D. Belaineh, J. W. Andreasen, J. Palisaitis, A. Malti, K. Håkansson, L. Wågberg, X. Crispin, I. Engquist and M. Berggren, *ACS Appl. Polym. Mater.*, 2019, **1**, 2342–2351.

32 A. Malti, J. Edberg, H. Granberg, Z. Ullah Khan, J. W. Andreasen, X. Liu, D. Zhao, H. Zhang, Y. Yao, J. W. Brill, I. Engquist, M. Fahlman, L. Wågberg, X. Crispin, M. A. Berggren Malti, J. Edberg, Z. U. Khan, D. Zhao, I. Engquist, X. Crispin, M. Berggren, H. Granberg, J. W. Andreasen, X. Liu, M. Fahlman, H. Zhang, Y. Yao, J. W. Brill and L. Wågberg, *Advanced Science*, 2016, **3**, 1500305.

33 J. Galvao, B. Davis, M. Tilley, E. Normando, M. R. Duchen and M. F. Cordeiro, *Faseb. J.*, 2014, **28**, 1317–1330.

34 S. Mabeau and J. Fleurence, *Trends Food Sci. Technol.*, 1993, **4**, 103–107.

35 R. S. Baghel, C. R. K. Reddy and R. P. Singh, *Carbohydr. Polym.*, 2021, **267**, 118241.

36 M. R. Moraes, A. C. Alves, F. Toptan, M. S. Martins, E. M. F. Vieira, A. J. Paleo, A. P. Souto, W. L. F. Santos, M. F. Esteves and A. Zille, *J. Mater. Chem. C*, 2017, **5**, 3807.

37 M. W. Lee, M. Y. Lee, J. C. Choi, J. S. Park and C. K. Song, *Org. Electron.*, 2010, **11**, 854–859.

38 X. Liu, J. Zai, A. Iqbal, M. Chen, N. Ali, R. Qi and X. Qian, *J. Colloid Interface Sci.*, 2020, **565**, 270–277.

39 S. H. Eom, S. Senthilarasu, P. Uthirakumar, S. C. Yoon, J. Lim, C. Lee, H. S. Lim, J. Lee and S. H. Lee, *Org. Electron.*, 2009, **10**, 536–542.

40 H. He, L. Zhang, S. Yue, S. Yu, J. Wei and J. Ouyang, *Macromolecules*, 2021, **54**, 1234–1242.

41 J. Ouyang, Q. Xu, C. W. Chu, Y. Yang, G. Li and J. Shinar, *Polym.*, 2004, **45**, 8443–8450.

42 A. Pasha, A. S. Roy, M. V. Murugendrappa, O. A. Al-Hartomy and S. Khasim, *J. Mater. Sci.: Mater. Electron.*, 2016, **27**, 8332–8339.

43 U. Heredia Rivera, S. Kadian, S. Nejati, J. White, S. Sedaghat, Z. Mutlu and R. Rahimi, *ACS Sens.*, 2022, **7**, 960–971.

44 A. Abedi, M. Hasanzadeh and L. Tayebi, *Mater. Chem. Phys.*, 2019, **237**, 121882.

45 S. Kongjao, S. Damronglerd and M. Hunsom, *Korean J. Chem. Eng.*, 2010, **27**, 944–949.

46 A. Gómez-Siurana, A. Marcilla, M. Beltrán, D. Berenguer, I. Martínez-Castellanos and S. Menargues, *Thermochim. Acta*, 2013, **573**, 146–157.

47 S. Singh, K. K. Gaikwad, S. Il Park and Y. S. Lee, *Int. J. Biol. Macromol.*, 2017, **99**, 506–510.

48 K. Madub, N. Goonoo, F. Gimié, I. Ait Arsa, H. Schönherr and A. Bhaw-Luximon, *Carbohydr. Polym.*, 2021, **251**, 117025.

49 B. Friedel, P. E. Keivanidis, T. J. K. Brenner, A. Abrusci, C. R. McNeill, R. H. Friend and N. C. Greenham, *Macromolecules*, 2009, **42**, 6741–6747.

50 J. H. Oh, G. W. George, A. D. Martinez, L. C. Moores and M. J. Green, *Polym.*, 2021, **230**, 124077.

51 V. Raman, A. R. Selvaraj, S.-W. Kim, K. Prabakar, H.-K. Kim, V. Raman, S.-W. Kim, H.-K. Kim, A. R. Selvaraj and K. Prabakar, *Adv. Electron. Mater.*, 2022, **8**, 2200504.

52 S. Ji, W. He, K. Wang, Y. Ran and C. Ye, *Small*, 2014, **10**, 4951–4960.

53 Y. Zhou, L. Zhao, Z. Song, C. Chang, L. Yang and S. Yu, *Opt. Mater.*, 2022, **126**, 112175.

54 J. W. Han, A. Prameswati, S. A. N. Entifar, J. H. Kim, A. F. Wibowo, J. Park, J. Lee, S. Kim, D. C. Lim, M. W. Moon, M. S. Kim and Y. H. Kim, *Electron. Mater. Lett.*, 2022, **18**, 532–539.

55 T. Bhargavi, N. M. Nair, A. Belavadi and P. Swaminathan, *IEEE J. Flex. Electron.*, 2022, 1.

56 E. Hosseini, N. Sabet, M. Arjmand, U. Sundararaj, H. Hassanzadeh, M. H. Zarifi and K. Karan, *Chem. Eng. J.*, 2022, **435**, 134598.

57 V. Raman, Y. H. Cho, H. M. Kim, Y. J. Kim, H. M. Sim and H. K. Kim, *Ceram. Int.*, 2021, **47**, 27230–27240.

58 K. Wang, X. Wang, J. Wang and F. Xiao, *2020 21st International Conference on Electronic Packaging Technology, ICEPT*, 2020, DOI: DOI: **10.1109/ICEPT50128.2020.9202551**.

59 N. M. Nair, J. K. Pakkathillam, K. Kumar, K. Arunachalam, D. Ray and P. Swaminathan, *ACS Appl. Electron. Mater.*, 2020, **2**, 1000–1010.

60 B. Hwang, A. Lund, Y. Tian, S. Darabi, S. Darabi and C. Müller, *ACS Appl. Mater. Interfaces*, 2020, **12**, 27537–27544.

61 X. Li, S. Yu, L. Zhao, M. Wu and H. Dong, *J. Mater. Sci.: Mater. Electron.*, 2020, **31**, 8106–8115.

62 X. He, G. Shen, R. Xu, W. Yang, C. Zhang, Z. Liu, B. Chen, J. Liu and M. Song, *Polymers*, 2019, **11**, 468.

63 J. Park, D. Han, S. Choi, Y. Kim and J. Kwak, *RSC Adv.*, 2019, **9**, 5731–5737.

64 M. Cao, M. Wang, L. Li, H. Qiu and Z. Yang, *ACS Appl. Mater. Interfaces*, 2018, **10**, 1077–1083.

65 X. He, R. He, Q. Lan, W. Wu, F. Duan, J. Xiao, M. Zhang, Q. Zeng, J. Wu and J. Liu, *Materials*, 2017, **10**, 220.

66 K. Hassan, N. Stanley, T. T. Tung, P. L. Yap, H. Rastin, L. Yu and D. Losic, *Adv. Mater. Interfaces*, 2021, **8**, 2101175.

67 A. S. Pillai, A. Chandran and S. K. Peethambharan, *Appl. Mater. Today*, 2021, **23**, 100987.

68 A. Ahmed, M. A. Jalil, M. M. Hossain, M. Moniruzzaman, B. Adak, M. T. Islam, M. S. Parvez and S. Mukhopadhyay, *J. Mater. Chem. C*, 2020, **8**, 16204–16215.

69 R. Zhou, P. Li, Z. Fan, D. Du and J. Ouyang, *J. Mater. Chem. C*, 2017, **5**, 1544–1551.

70 K. Pattanarat, N. Petchsang, T. Osotchan, Y. H. Kim and R. Jaisutti, *ACS Appl. Mater. Interfaces*, 2021, **13**, 48053–48060.

71 Z. R. Ramadhan, J. W. Han, J. Hong, S. Bin Park, J. H. Kim, A. F. Wibowo, A. Prameswati, S. Y. Kim, J. Lee, S. Kim, D. Chan Lim, M. W. Moon, M. S. Kim and Y. H. Kim, *Org. Electron.*, 2021, **94**, 106165.

72 I. S. Jin, J. U. Lee and J. W. Jung, *Polymers*, 2021, **13**, 945.

73 J. Lee, H. Kwon, J. Seo, A. M. Basodan, B. Park, H.-J. Chung, I. Su Jin, W. Lee, S. Ju Lim, J. Hoon Ko and J. Woong Jung, *Smart Mater. Struct.*, 2020, **29**, 095002.

74 J. Zhou, M. Mulle, Y. Zhang, X. Xu, E. Q. Li, F. Han, S. T. Thoroddsen and G. Lubineau, *J. Mater. Chem. C*, 2016, **4**, 1238–1249.

75 C. Yeon, G. Kim, J. W. Lim and S. J. Yun, *RSC Adv.*, 2017, **7**, 5888–5897.